arXiv:1301.3802v1 [cond-mat.mes-hall] 16 Jan 2013

Solitons in a composite multiferroic chain

L. Chotorlishvili[1], R. Khomeriki[2,3], A. Sukhov[1], S. Ruffo[4] and J. Berakdar[1]
[1] *Institut für Physik, Martin-Luther Universität Halle-Wittenberg, D-06120 Halle/Saale, Germany*
[2] *Physics Department, Tbilisi State University, 0128 Tbilisi, Georgia*
[2] *Max-Planck Institute for the Physics of Complex Systems, Nöthnitzer Str. 38, 01187 Dresden, Germany*
[4] *Dipartimento di Energetica "Sergio Stecco" and CSDC,*
Università di Firenze and INFN, 50139 Firenze, Italy

(Dated: January 17, 2013)

In a coupled ferroelectric/ferromagnetic system, i.e. a composite multiferroic, the propagation of magnetic or ferroelectric excitations across the whole structure is a key issue for applications. Of a special interest is the magnetic or ferroelectric soliton dynamics across the ferroelectric-ferromagnetic interface, particularly when the soliton carrier frequency is in the band of the ferroelectric and in the band gap of the ferromagnet. For a proper choice of system parameters, we find that there is a threshold amplitude above which the interface becomes transparent and a band gap ferroelectric soliton penetrates the ferromagnetic array. Below that threshold the soliton is fully reflected. Slightly below the transmission threshold, the addition of noise may lead to soliton transmission, provided that the noise level is not too low or too high, as found in stochastic resonance. These findings represent an important step towards the application of ferroelectric and/or ferromagnetic soliton-based logic.

PACS numbers: 85.80.Jm, 75.78.-n, 77.80.Fm

Introduction.- The revival of research on multiferroics (MF), *i.e.* systems with coupled ferroic (magnetic, electric, or elastic) orders [1–3] is fueled by recent advances in synthesizing composite ferroelectric (FE)/ferromagnetic (FM) nano and multi layer structures that show a substantially larger multiferroic coupling strength [1–5] as compared to bulk matter, i.e. single-phase multiferroics [6, 7] such as Cr_2O_3[8]. MF are important for addressing fundamental questions regarding the cross correlation between electronic correlation, symmetry, magnetism, and polarization but also hold the promise for qualitatively new device concepts that exploit magnetoelectric (ME) coupling to steer magnetism (ferroelectricity) via electric (magnetic) fields. Potential applications are wide ranging from sensorics and magnetoelectric spintronics to environmentally friendly devices with ultra low heat dissipation [9–11]. Thereby, a key issue is how efficient magnetic or ferroelectric information, i.e. an initial excitation, is transmitted in a system with a MF coupling. For instance, in a two-phase or composite MF [6, 7, 12] such as $BaTiO_3/CoFe_2O_4$ [13], $PbZr_{1-x}Ti_xO_3$/ferrites [14, 15], $BaTiO_3$/Fe [16], $PbTiO_3$/Fe [17, 18] or $BaTiO_3$/Ni the MF coupling is strongest at the FE/FM interface whereas away from it the FE or FM order is only marginally affected. We expect, thus that a ferroelectric signal triggered by an electric field in the FE part may or may not be converted into a magnetic signal depending on the dynamics taking place at the interface. How this transport of information depends on the properties of the system is rarely studied and will be addressed in this work. The outcome of such a study would not only uncover the conditions for optimal signal handling but also holds the potential for new insights into the mutliferroic coupling retrieved by tracing the signal dynamics. We will focus on nonlinear waves forming solitons that are known, in the pure FM or FE phase, to have a series of applications in magnetic logic, microwave signal processing, and spin electronic devices. Advantageous in this respect is that solitons (i.e. localized state of a large number of elementary excitations, e.g. magnons) are very robust and have a particle-like nature [19]. Hence, logic operation based on magnetic soliton attracted detailed considerations [20, 21]. Multiferroics offer new fascinating mechanisms for the soliton dynamics. For example, due to discreteness and/or nonlinearity of the system, it may happen that the frequency of the large amplitude excitation may fall within the gap of the linear oscillations

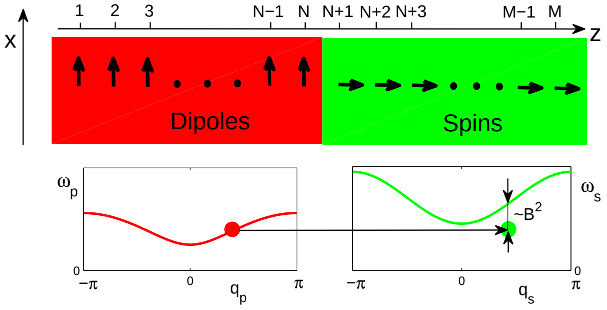

FIG. 1. (color online) Schematics of a chain consisting of ferroelectric and ferromagnetic parts coupled at the interface. Lower panel shows a particular choice of frequency for which in the ferroelectric a conventional envelope soliton is formed, while in ferromagnetic part bandgap soliton develops with a nonlinear frequency shift proportional to B^2 (B is an amplitude of magnetic gap-soliton). The chosen mutual alignment of the ferroelectric polarization and the magnetization at the interface resembles the realized ferroelectric ($BaTiO_3$) tunnel junction with ferromagnetic (Fe) electrodes [22].

spectrum, as illustrated in Fig.1. Therefore, the energy of the excitation would not spread over the lattice. As well established from detailed studies on intrinsic localized modes, e.g. [23–30], we know that in spite of the localized energy profile, such modes may move along the whole chain. This means that excitations created in the ferroelectric part via an electric field can be transmitted to the magnetic part and move there. Moreover, as it will be shown below the creation of these band-gap localizations could be enhanced by the noise manifesting thus some analogy with stochastic resonance phenomenon [31, 32].

Model.- For our purposes a large ME coupling is necessary. In this regard, new fabrication methods [15] for so-called two-phase or composite multiferroics [6, 7, 12] as well as the realization of ferroelectric wires [33] are encouraging. Examples of composite multiferroics $\mathrm{BaTiO_3/CoFe_2O_4}$ [13] or $\mathrm{PbZr_{1-x}Ti_xO_3}$/ferrites [15] are still popular. Major research is focused on $\mathrm{BaTiO_3}$/Fe [16], $\mathrm{PbTiO_3}$/Fe [17, 18] or $\mathrm{BaTiO_3}$/Ni composite multiferroics, to name but a few, since their bulk parameters are very well known (Ref. [34] for $\mathrm{BaTiO_3}$ and Ref. [35] for Fe or Ni) as well as the misfit of lattices is relatively low [17]. Relatively high ME constants [17, 18] were predicted for these materials at room temperatures. A possible mechanism for ME coupling at the FE/FM interface, that is also assumed here, is based on screening effects [36]: In the polarized FE layer surface charges are created which are compensated by screening charges in the metallic FM electrodes when attached to the FE layer. In this heterostructure the accumulated screening charge density on the FM side of the interface is spin-polarized and couples then to the magnetization in FM. Technically, we describe the bulk unstrained $\mathrm{BaTiO_3}$ by the Ginzburg-Landau-Devonshire potential FGLD [34]. For the discretized FE polarization (P_n) in a coarse-grained approach, the form of the FGLD potential for a general phase and arbitrary temperatures is quite involved [37]. However, at room temperature $\mathrm{BaTiO_3}$-crystal has an axis along which the polarization switches (tetragonal phase). Consequently, the form of the FGLD potential reduces to the one dimensional biquadratic potential. For the description of the magnetization dynamics in iron (Fe) (S_k, discretized and normalized to the saturation value of the coarse-grained magnetization vector), we employ the classical Heisenberg model. With the aim to explore the feasibility of conversion of the electric excitation formed in FE part into a localized spin magnetic excitation in FM part we employ thus the multiferroic model (cf. Fig. 1)

$$H = H_{\mathrm{P}} + H_{\mathrm{S}} + V_{\mathrm{SP}}, \tag{1}$$

$$H_{\mathrm{P}} = \sum_{n=1}^{N} \left(\tfrac{\alpha_0}{2} \dot{P}_n^2 + \tfrac{\alpha_1}{2} P_n^2 + \tfrac{\alpha_2}{4} P_n^4 + \tfrac{\kappa}{2} \left(P_{n+1} - P_n\right)^2 \right),$$

$$H_{\mathrm{S}} = \sum_{k=N+1}^{M} \left(-J_1 \vec{S}_k \vec{S}_{k+1} - J_2 \left(S_k^z\right)^2 \right), \quad V_{\mathrm{SP}} = -g P_N S_1^x,$$

where H_{P} is the Hamiltonian of FE part for the multiferroic system of N-interacting FE dipole [29, 37] P_n. Note, that at room temperature, the polarization vector has only one nonzero component and we choose the polarization vector to be directed along the x axis $\vec{P_n} = (P_n, 0, 0)$, $n = 1, \ldots, N$. α_0 is a kinetic coefficient, $\alpha_{1,2}$ define the FGLD potential constants and κ is the nearest neighbor coupling constant. H_{S} is the classical Hamiltonian of the ferromagnetic part of the system [38], where J is the nearest neighbor exchange coupling in the FM part. The coarse-grained FM order parameters are $\vec{S}_k$, $k = N+1, \ldots, M$ and D is the uniaxial anisotropy constant. Interface effects between the spin and the FE dipole systems are described by the dipole-spin interaction Hamiltonian V_{SP}. Since we assume the ME coupling to be due to screening and the screening constant in metals is on the scale of the lattice constant we couple only the (coarse grained) dipole at the interface (indexed N) to the interfacial spin (with index 1).

In our numerical simulations we will operate with dimensionless quantities upon introducing $p_n = P_n/P_{max}$, $\vec{s}_k = \vec{S}_k/S$ and defining a dimensionless time as $t \to \omega_0 t$ ($\omega_0 = \sqrt{\kappa/\alpha_0} \sim 10^{12}$ Hz). The equations governing the time evolution of the dipoles and the spins (except for the sites near the interface) read

$$\frac{d^2 p_n}{dt^2} = -\alpha p_n - \beta p_n^3 + \left(p_{n-1} - 2p_n + p_{n+1}\right) \tag{2}$$

$$\frac{\partial s_k^{\pm}}{\partial t} = \pm i J \left[s_k^{\pm} \left(s_{k-1}^z + s_{k+1}^z \right) - s_k^z \left(s_{k-1}^{\pm} + s_{k+1}^{\pm} \right) \right] \pm \\ \pm 2iD s_k^{\pm} s_k^z \tag{3}$$

where $n \neq N$ and $k \neq N+1$. We introduced the following dimensionless constants $\alpha = \alpha_1/\kappa$, $\beta = \alpha_2 P_{max}^2/\kappa$, $J = J_1 S/\omega_0$ and $D = J_2 S/\omega_0$. For the dipole p_N and the spin $\vec{s}_1$ at the interface the relation applies

$$\frac{d^2 p_N}{dt^2} = -\alpha p_N - \beta p_N^3 + \left(p_{N-1} - 2p_N + g_s s_1^x\right) \tag{4}$$

$$\frac{\partial s_1^{\pm}}{\partial t} = \pm i J \left[s_1^{\pm} s_2^z - s_1^z s_2^{\pm} \right] \pm i \left[2D s_1^{\pm} s_1^z - g_p p_N s_1^z \right].$$

Here $s_k^{\pm} \equiv s_k^x \pm i s_k^y$, $g_s = gS/(\kappa P_{max})$ and $g_p = g P_{max}/(S\omega_0)$. The evolution according to Eqs. (2-4) proceeds under the constraint $\left(s_k^x\right)^2 + \left(s_k^y\right)^2 + \left(s_k^z\right)^2 = 1$.

For the derivation of weakly nonlinear envelope solutions from eqs. (2) and (3) one can utilize the reductive perturbation theory developed in Ref. [39, 40] and obtain the solutions for the dipoles and spins separately in the following form (a detailed derivation is provided as supplementary materials to this paper):

$$p_n = \frac{A \cos\left[\omega_p t - q_p n + \delta\omega_p t\right]}{\cosh\left[(n - V_p t)/\Lambda_p\right]} \quad s_k^{\pm} = \frac{B e^{\pm i(\omega_s t - q_s k + \delta\omega_s t)}}{\cosh\left[(k - V_s t)/\Lambda_s\right]} \tag{5}$$

where A and B are the amplitudes of the dipolar and the magnetic envelope solitons, respectively; ω_p and ω_s are the frequencies of the linear excitations which obey the following dispersion relations

$$\omega_p = \sqrt{\alpha + 2\,(1-\cos q_p)}, \quad \omega_s = 2\,[D + J(1-\cos q_s)]\,, \tag{6}$$

q_p and q_s are the carrier wave numbers of the dipolar and the spin excitations; $V_p = \sin q_p/\omega_p$ and $V_s = 2J\sin q_s$ are the group velocities of the corresponding solitons. The width of the dipolar and spin solitons are

$$\Lambda_p = \frac{1}{A}\sqrt{\frac{2\left(\omega_p^4 - \alpha^2 - 4\alpha\right)}{3\omega_p^2\beta}}, \quad \Lambda_s = \frac{1}{B}\sqrt{\frac{4J\cos q_s}{\omega_s}}. \tag{7}$$

The nonlinear frequency shifts are defined as

$$\delta\omega_p = A^2\frac{3\beta}{16\omega_p}, \qquad \delta\omega_s = -B^2\frac{\omega_s}{4}. \tag{8}$$

At first we note that for the wave packet transmission the matching condition between the frequencies has to be fulfilled

$$\omega_p + \delta\omega_p = \omega_s + \delta\omega_s. \tag{9}$$

In addition, for an efficient transmission of the soliton from FE into FM part the widths of the solitons should be the same in both parts, i.e. $\Lambda_p = \Lambda_s$ with the restriction $B \le g_p A$. If one excites the soliton with a carrier frequency ω which is located within the band of both the dipolar and the spin wave spectrum, then the soliton will safely penetrate from the FE to the FM part, but some portion of the energy will be reflected from the interface. Changing the soliton amplitude one can manipulate the ratio between the transmitted and reflected parts. In addition, the transmission is very sensitive to the coupling constant g between FE and FM parts. We have investigated this dependence by fixing the values for the dimensionless parameters as follows: $\alpha = 0.2$; $\beta = 0.1$; $J = 1$; $D = 0.6$ and varying the coupling constant g_s. We assume for simplicity $g_p = g_s$ (in general these constants differ depending on the samples material but present no obstacles for theory).

Numerical Results.- Graphs a), b), c) of Fig. 2 show the localized energy evolution along the lattice for different values of coupling constant g_p. In graph d) the dependence of transmitted energy on the coupling constant is displayed evidencing that the transmission is maximal when g_p lays in between the spin coupling constant $J = 0.5$ and dipolar coupling constant (in reduced units it is equal to 1). An insight into the spins alignment as well as the topology of the excitation and its propagation in the chain's FM part at different time moments is displayed graphically in the supplementary material to this paper.

Further interesting effects arise when a band soliton forms having a carrier frequency ω located in the band of the dipolar spectrum (see bottom panel of Fig. 1) and slightly below the zone boundary $\omega_s(q_s = 0)$ of spin wave spectrum. Then for small amplitudes the dipolar soliton is totally reflected from the interface because it does not resonate with any mode in the spin array. However with increasing the amplitude, there is a threshold value A_{cr} (due to the nonlinear frequency shift) above which the soliton starts to transmit towards the FM part of the multiferroic chain forming thus a magnetic gap soliton. Using Eqs. (8) and (9) and assuming $B = A$ one can infer the relation defining this threshold amplitude to be

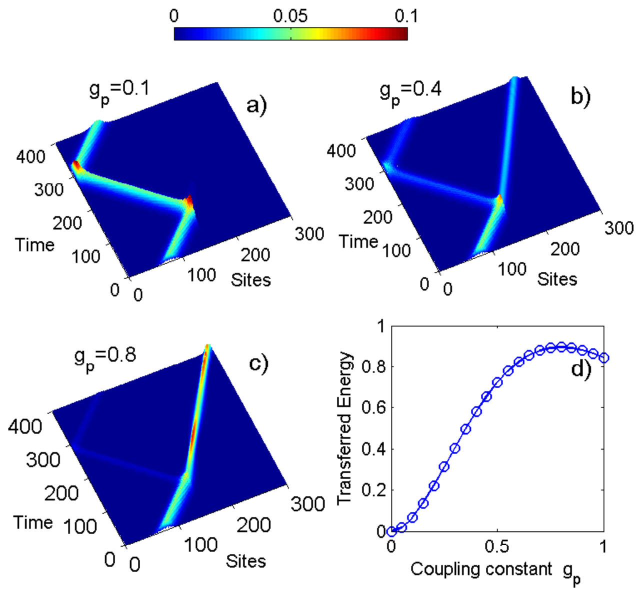

FIG. 2. (color online) Insets a), b) and c) show the dependence of the local energy (for dipoles it is given by the local values of $H_{\rm P}$ and for spins it is obtained from the local values of the expression $H_{\rm S} + S^2[J_1 + J_2]$) on the site number and the simulation times as dictated by Eqs. (2)-(4) for the set of parameters given in the text and for the different values of coupling constant g_p that are indicated in the graphs ($g_p \propto g$ and g is the interfance ME coupling strength). The dipolar soliton carrier wave number is chosen as $q_p = 0.4\pi$ and the dipolar soliton amplitude is chosen as $A = 0.2$. Dipoles and spins are occupying the sites $n = 1\ldots150$ and $k = 151\ldots300$, respectively. d) The dependence of the relative energy transferred to FM part (i.e. the ratio of the energy in FM part on the whole injected energy) on the coupling constant strength g_p.

$$\omega_s(q_s = 0) - \omega = \left(\frac{g_p^2\omega}{4} + \frac{3\beta}{16\omega}\right)A_{cr}^2. \tag{10}$$

Based on this observation, we proceed with the simulations according to Eqs. (2)-(4) with the set of parameters given above and choosing $g_p = g_s = 1$ and starting at $t = 0$ with a soliton in the form of the first expression in Eq. (5) with a carrier wave number $q_p = 0.37$. For such a wave number the corresponding linear frequency is $\omega = 1.1856$ thus it is located in the band gap of the spin wave spectrum and no soliton transmission happens in the case of small amplitudes as it is seen from graph a)

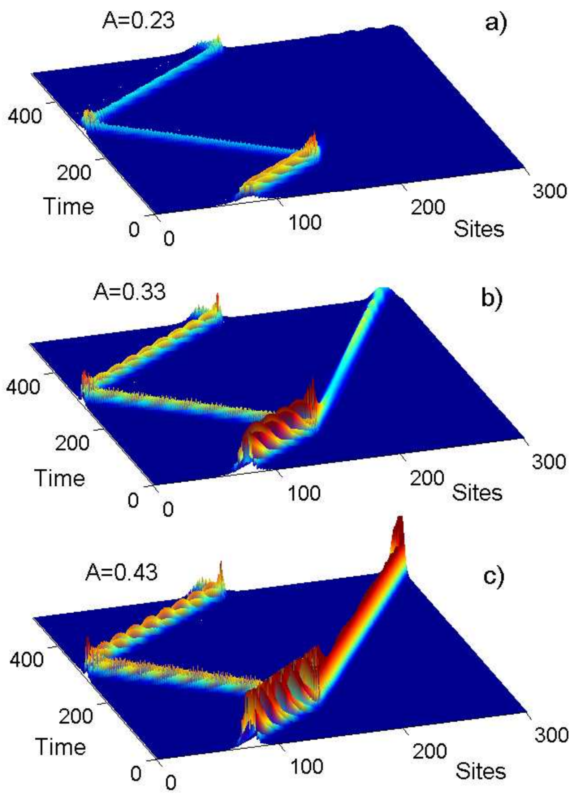

FIG. 3. (color online) The same as in graphs a)-c) of Fig. 2 for the set of parameters given in the text and $g_p = g_s = 1$. The dipolar soliton carrier wave number is chosen as $q_p = 0.37\pi$ and the dipolar soliton amplitude values are indicated in the graphs. Color scale as in Fig. 2.

of Fig. 3. According to the relation (10) we can calculate the threshold amplitude for which a soliton transmission emerges and find $A_{cr} = 0.22$. In the numerical results the transmission occurs for the incident soliton amplitudes $A > 0.27$. This discrepancy is explained by the fact that the solitons amplitudes in different parts of multiferroic structure does not exactly coincide. In the graph b) of Fig. 2 we display the dynamics for a larger soliton amplitude, i.e. $A = 0.33$ and find that an envelope soliton is formed in the ferromagnetic part as well. With further increasing the soliton amplitude, the transmitted soliton takes over almost all the energy of the incident one (graph c) of the same figure).

keeping the amplitude of the incident soliton slightly below the threshold (in our simulations we choose $A = 0.265$) it is obvious that even a small perturbation may cause transmission to FM part. Thus we add a term $\vec{f}(t)\vec{S}_1$ to the Hamiltonian (2) describing the action of a random magnetic field at the interface spins. $f(t)$ is uncorrelated in time and randomly distributed in the interval $[-f, f]$. Then for small random fields $f = 0.05$ the picture is almost the same as in the case of a zero noise (please compare upper graphs of Figs. 3 and 4).

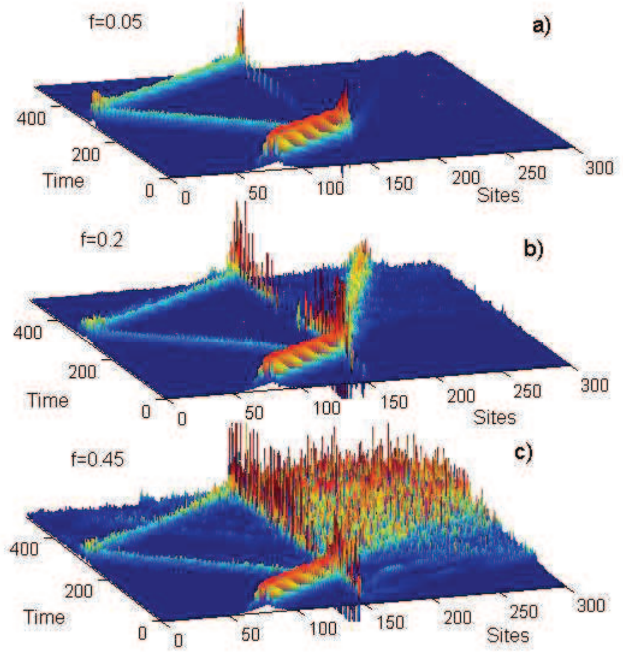

FIG. 4. (color online) The same as in Fig. 3 (including the color scale), however with a fixed soliton amplitude $A = 0.265$ and different noise levels indicated in the graphs.

Increasing the noise strength to a moderate level, energy transmission in FM part takes place (see graph b) of Fig. 4). This stochastic resonance like behavior is displayed in graph c) of the Fig. 4.

Summary.- As evidenced by analytical and numerical results, in a two-phase multiferroic the magnetoelectric coupling at the interface renders possible the conversion of an initial ferrolectric soliton into a ferromagnetic signal, opening thus the door for FE and/or FM soliton-based logic in multiferroics. As an essential step in this direction we identified the conditions under which a FE signal is converted into a FM one and clarified the role of noise.

Acknowledgements.- Consultations with Marin Alexe on the experimental realization are gratefully acknowledged. L.Ch., A.S. and J.B. are supported by DFG through SU 690/1-1 and SFB 762. R.Kh. and S.R are funded by a joint Grant from French CNRS and Georgian RNSF (Grant No 09/08).

---

[1] W. Eerenstein, N. D. Mathur, and J. F. Scott, Nature **442** (2006) 759.
[2] Y. Tokura and S. Seki, Adv. Mater. **22** (2010) 1554 .
[3] Carlos A. F. Vaz, Jason Hoffman, Charles H. Ahn, and Ramamoorthy Ramesh, Adv. Meter. **22** (2010) 2900.
[4] F. Zavaliche, T. Zhao, H. Zheng, F. Straub, M. P. Cruz,

P.-L. Yang, D. Hao, and R. Ramesh, Nano. Lett. **7** (2007) 1586.

[5] H.L. Meyerheim, F. Klimenta, A. Ernst, K. Mohseni, S. Ostanin, M. Fechner, S. Parihar, I.V. Maznichenko, I. Mertig, and J. Kirschner, Phys. Rev. Lett. **106** (2011) 087203.

[6] W. Eerenstein, N.D. Mathur, J.F. Scott, Nature **442**, 759 (2006).

[7] R. Ramesh, N.A. Spaldin, Nat. Mater. **6**, 21 (2007).

[8] I.E. Dzyaloshinkskii, Sov. Phys. JETP **10**, 628 (1959).

[9] M. Bibes and A. Barthélémy, Nature Mater. **7** (2008) 425 .

[10] M. Gajek, M. Bibe, S. Fusil, K. Bouzehouane, J. Fontcuberta, A. Barthélémy, and A. Fert, Nature Mater. **6** (2007) 296.

[11] D. Pantel, S. Goetze, D. Hesse and M. Alexe, Nature Mater. **11** (2012) 289.

[12] C.-W. Nan, M.I. Bichurin, S. Dong, D. Viehland, G. Srinivasan, J. Appl. Phys. **103**, 031101 (2008).

[13] J. van den Boomgaard, A.M.J.G. van Run, and J. van Suchtelen, Ferroelectrics **10**, 295 (1976).

[14] N. Spaldin, M. Fiebig, Science **309**, 391 (2005).

[15] M. Fiebig, J. Phys. D: Appl. Phys. **38**, R123 (2005).

[16] C.-G. Duan, S.S. Jaswal, E.Y. Tsymbal, Phys. Rev. Lett. **97**, 047201 (2006).

[17] M. Fechner, I.V. Maznichenko, S. Ostanin, A. Ernst, J. Henk, I. Mertig, Phys. Stat. Solidi B **247**, 1600 (2010).

[18] J.-W. Lee, N. Sai, T. Cai, Q. Niu, A.A. Demkov, Phys. Rev. B **81**, 144425 (2010).

[19] A. M. Kosevich, B. A. Ivanov and A. S. Kovalev, Phys. Rep. 194 117, (1990).

[20] R. P. Cowburn and M. E. Welland, Science 287, 1466 (2000); R. P. Cowburn and M. E. Welland, Appl. Phys. Lett. **72**, 2041 (1998).

[21] P. Wadhwa and M. B. A. Jalil, Appl. Phys. Lett. **85**, 2367 (2004).

[22] V. Garcia, M. Bibes, L. Bocher, S. Valencia, F. Kronast, A. Crassous, X. Moya, S. Enouz-Vedrenne, A. Gloter, D. Imhoff, C. Deranlot, N.D. Mathur, S. Fusil, K. Bouzehouane, A. Barthélémy, Science **327**, 1106 (2010).

[23] B.I. Swanson, J.A. Brozik, S.P. Love, G.F. Strouse, A.P. Shreve, A.R. Bishop, W.Z. Wang, M.I. Salkola, Phys. Rev. Lett. **82**, 3288 (1999).

[24] U.T. Schwarz, L.Q. English, A.J. Sievers, Phys. Rev. Lett. **83**, 223 (1999).

[25] G. Kopidakis, S. Aubry, G.P. Tsironis, Phys. Rev. Lett. **87**, 165501 (2001).

[26] S. Flach, K. Kladko, Physica D **127**, 61 (1999).

[27] A.K. Bandyopadhyay, P.C. Ray, V. Gopalan, J. Phys.: Condens. Matter **18**, 4093 (2006).

[28] P. Giri, K. Choudhary, A. Sengupta, A.K. Bandyopadhyay, P.C. Ray, J. Appl. Phys. **109**, 054105 (2011).

[29] P. Giri, K. Choudhary, A.S. Gupta, A.K. Bandyopadhyay, A.R. McGurn, Phys. Rev. B **84**, 155429 (2011).

[30] A.K. Bandyopadhyay, P.C. Ray, L. Vu-Quoc, A.R. McGurn, Phys. Rev. B **81**, 064104 (2010).

[31] R. Benzi, A. Sutera, A. Vulpani, J. Phys.: Math. Gen. **14**, L453 (1981).

[32] L. Gammaitoni, P. Hänggi, P. Jung, F. Marchesoni, Rev. Mod. Phys. **70**, 224 (1998).

[33] M. Alexe, and D. Hesse, Ferroelectrics **433**, 53 (2012).

[34] *Physics of Ferroelectrics*, K. Rabe, Ch. H. Ahn and J.-M. Triscone (Eds.), (Springer, Berlin 2007).

[35] *Magnetism and magnetic materials*, J.M.D. Coey, (Cambridge University Press, Cambridge 2010).

[36] T. Cai, S. Ju, J. Lee, N. Sai, A. A. Demkov, Q. Niu, Z. Li, J. Shi, and E. Wang, Phys. Rev. B **80**, 140415(R) (2009).

[37] A. Sukhov, C.-L. Jia, P.P. Horley, and J. Berakdar, J. Phys.: Cond. Matt. **22**, 352201 (2010); Phys. Rev. B **85**, 054401 (2012); EPL **99**, 17004 (2012); Ferroelectrics **428**, 109 (2012); J. Appl. Phys. at press (2013).

[38] *Physics of Ferromagnetism*, S. Chikazumi, (Oxford University Press Inc., New York 2002).

[39] M. Oikawa, N. Yajima, Progr. Theor. Phys. **55**, 36 (1974).

[40] N. Giorgadze, R. Khomeriki, Phys. Stat. Sol. (b), **207**, 249, (1998).

SUPPLEMENTARY MATERIAL

As an additional detail to figure 2 of the main text, Fig.5 provides an insight into the real space spin alignments and their time evolution for the same parameters discussed for figure 2 of the main text.

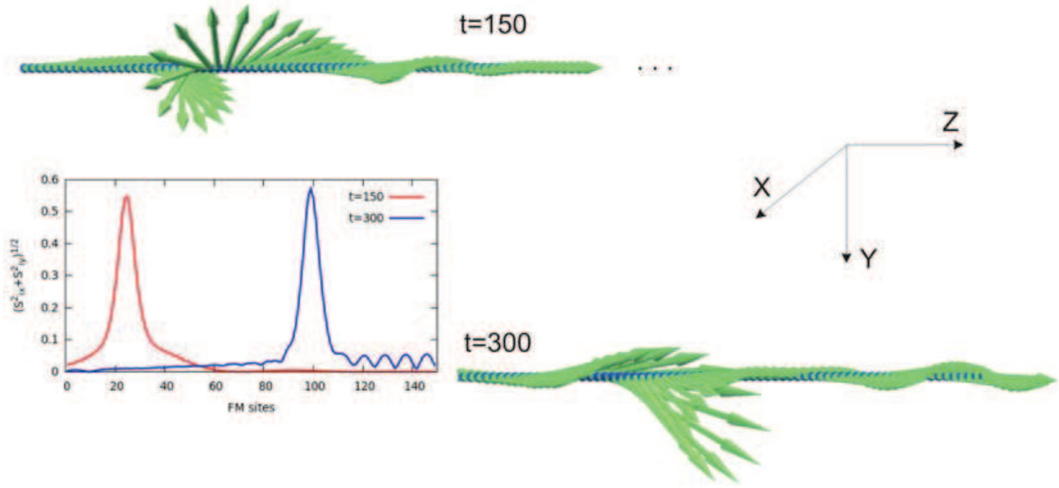

FIG. 5. (color online) The real space spin configuration in the FM part of the chain at certain time moments ($t = 150$ and $t = 300$ in normalized units) displayed for the for the case depicted in Fig. 2(c) in the main text. $\sqrt{s_{ix}^2 + s_{iy}^2}$ at the sites i of the FM chain is also shown.

MATHEMATICAL DETAILS

A solution method for Eq.(2) of the main text is needed. This equation reads

$$\frac{d^2 p_n}{dt^2} = -\alpha p_n - \beta p_n^3 + (p_{n-1} - 2p_n + p_{n+1}) \qquad (11)$$

which describes the FE dynamics that we capture via the reductive perturbation method [39] that builds on a multiple scale expansion in the following form

$$p_n = \sum_{\alpha=1}^{\infty} \varepsilon^{\alpha} \sum_{m=-\infty}^{\infty} \Psi_m^{(\alpha)}(\xi,\tau)\, e^{im(\omega t - qn)}, \qquad (12)$$

where $\Psi_m^{(\alpha)} = \left(\Psi_{-m}^{(\alpha)}\right)^*$ and the slow variables are

$$\xi = \varepsilon(n - Vt), \qquad \tau = \varepsilon^2 t. \qquad (13)$$

We insert (12) into the initial equation (11) and keep the expansion terms up to the third order over ε. For this the following derivative over time is needed

$$\frac{\partial}{\partial t}\Psi_m^{(\alpha)} = -\varepsilon V \frac{\partial}{\partial \xi}\Psi_m^{(\alpha)} + \varepsilon^2 \frac{\partial}{\partial \tau}\Psi_m^{(\alpha)}. \qquad (14)$$

Furthermore we make the reduction of p_{n+1} and p_{n-1}

$$p_{n\pm1} = \sum_{\alpha=1}^{\infty} \varepsilon^{\alpha} \sum_{m=-\infty}^{\infty} \Psi_m^{(\alpha)}(\xi \pm \varepsilon, \tau)\, e^{im(\omega t - qn \mp q)}, \qquad (15)$$

and perform the expansion of $\Psi_m^{(\alpha)}(\xi \pm \varepsilon, \tau)$ in terms of small ε. We recall also that only terms up to third order over ε need to be kept. Then we obtain the following expressions for p_n and $p_{n\pm1}$

$$\begin{aligned} p_n &= \sum_{m=-\infty}^{\infty} \left(\varepsilon\Psi_m^{(1)} + \varepsilon^2\Psi_m^{(2)} + \varepsilon^3\Psi_m^{(3)}\right) e^{im(\omega t - qn)}, \\ p_{n\pm1} &= \sum_{m=-\infty}^{\infty} \Bigg(\varepsilon\Psi_m^{(1)} + \varepsilon^2\left[\Psi_m^{(2)} \pm \tfrac{\partial\Psi_m^{(1)}}{\partial\xi}\right] + \qquad (16) \\ &\quad + \varepsilon^3\left[\Psi_m^{(3)} \pm \tfrac{\partial\Psi_m^{(2)}}{\partial\xi} + \tfrac{\partial^2\Psi_m^{(1)}}{\partial\xi^2}\right]\Bigg) e^{im(\omega t - qn \mp q)}. \end{aligned}$$

Inserting these into Eq.(11) and taking into account the relation (14) for the time derivative we obtain to a first approximation with respect to ε the following relation

$$\varepsilon \sum_{m=-\infty}^{\infty} e^{im(\omega t-qn)} \left[\omega^2 m^2 - \alpha + \left(e^{imq} + e^{-imq} - 2\right)\right] \Psi_m^{(1)} = 0. \tag{17}$$

Let us assume that $\Psi_{\pm1}^{(1)}$ is nonzero. From this the dispersion relation follows straightforwardly

$$\omega^2 = \alpha + 2(1 - \cos q) \tag{18}$$

and all other $\Psi_m^{(1)}$ with $m \neq \pm 1$ are exactly zero.

In the second approximation one has the relation

$$\varepsilon^2 \sum_{m=-\infty}^{\infty} e^{im(\omega t-qn)} \left[\omega^2 m^2 - \alpha + \left(e^{imq} + e^{-imq} - 2\right)\right] \Psi_m^{(2)} + \varepsilon^2 \sum_{m=-\infty}^{\infty} e^{im(\omega t-qn)} \left[2i\omega m V + \left(e^{-imq} - e^{imq}\right)\right] \frac{\partial \Psi_m^{(1)}}{\partial \xi} = 0. \tag{19}$$

From the dispersion (18) and the fact that all $\Psi_m^{(1)}$ with $m \neq \pm 1$ are zero it follows that $\Psi_m^{(2)}$ with $m \neq \pm 1$ are zero as well and one has the second relation defining velocity V

$$V = \sin q / \omega \tag{20}$$

Finally in the third approximation with regard to ε we find

$$-\left(\beta p_n^3\right)\big|_{\varepsilon^3} + \varepsilon^3 \sum_{m=-\infty}^{\infty} e^{im(\omega t-qn)} \Big\{ \left[\omega^2 m^2 - \alpha + \left(e^{imq} + e^{-imq} - 2\right)\right] \Psi_m^{(3)} + \tfrac{1}{2}\left(-2V^2 + e^{imq} + e^{-imq}\right) \tfrac{\partial^2 \Psi_m^{(1)}}{\partial \xi^2} + \left(2i\omega m V + e^{-imq} - e^{imq}\right) \tfrac{\partial \Psi_m^{(2)}}{\partial \xi} - 2im\omega \tfrac{\partial \Psi_m^{(1)}}{\partial \tau} \Big\} = 0 \tag{21}$$

where the nonlinear term in the third approximation reads

$$-\left(\beta p_n^3\right)\big|_{\varepsilon^3} = -\varepsilon^3 \beta \left\{ \left(\Psi_1^{(1)}\right)^3 e^{3i(\omega t-qn)} + \left(\Psi_1^{*(1)}\right)^3 e^{-3i(\omega t-qn)} + 3\left|\Psi_1^{(1)}\right|^2 \left(\Psi_1^{(1)} e^{i(\omega t-qn)} + \Psi_1^{*(1)} e^{-i(\omega t-qn)}\right) \right\} \tag{22}$$

Collecting the terms proportional to $e^{i(\omega t-qn)}$ (meaning that we choose the harmonics with $m = 1$) and taking into account the relations (18) and (20) we obtain

$$i\frac{\partial \Psi_1^{(1)}}{\partial \tau} + \frac{\omega^4 - \alpha^2 - 4\alpha}{8\omega^3} \frac{\partial^2 \Psi_1^{(1)}}{\partial \xi^2} + \frac{3\beta}{2\omega} \left|\Psi_1^{(1)}\right|^2 \Psi_1^{(1)} = 0. \tag{23}$$

One soliton solution of the nonlinear Schrödinger equation (23) can be written in the form

$$\Psi_1^{(1)} = \exp\left[i\frac{3\beta}{4\omega}\tau\right] \Big/ \cosh\left[\xi\sqrt{\frac{6\omega^2\beta}{\omega^4 - \alpha^2 - 4\alpha}}\right] \tag{24}$$

and thus in the first approximation over ε we find the following expression for the coupled dipoles according to the expansion (12)

$$p_n = 2\varepsilon \cos\left[\omega t - pn + \varepsilon^2 \frac{3\beta}{4\omega} t\right] \Big/ \cosh\left[\varepsilon(n - Vt)\sqrt{\frac{6\omega^2\beta}{\omega^4 - \alpha^2 - 4\alpha}}\right] \tag{25}$$

or assuming, that the amplitude is defined as $A = 2\varepsilon$

$$p_n = A \cos\left[\omega t - pn + A^2 \frac{3\beta}{16\omega} t\right] \Big/ \cosh\left[A(n - Vt)\sqrt{\frac{3\omega^2\beta}{2\left(\omega^4 - \alpha^2 - 4\alpha\right)}}\right] \tag{26}$$

which is the same as the first expression in Eq.(5) with the definitions Eqs.(7) and (8) of the main text.

For the spins we rewrite the equation Eq.(3) of the main text

$$\frac{ds_k^{\pm}}{dt} = \pm iJ\left[s_k^{\pm}\left(s_{k-1}^z + s_{k+1}^z\right) - s_k^z\left(s_{k-1}^{\pm} + s_{k+1}^{\pm}\right)\right] \pm 2iDs_k^{\pm}s_k^z \tag{27}$$

where the z spin component is defined from the relation $s_k^+ s_k^- + \left(s_k^z\right)^2 = 1$. We proceed again with the similar expansion as in the dipolar case

$$s_k^+ = \sum_{\alpha=1}^{\infty} \varepsilon^{\alpha} \sum_{m=-\infty}^{\infty} \Psi_m^{(\alpha)}\left(\xi,\tau\right) e^{im(\omega t - qk)}, \qquad s_k^z = 1 - \frac{s_k^+ s_k^-}{2}, \qquad \xi = \varepsilon(k - Vt), \qquad \tau = \varepsilon^2 t \tag{28}$$

Substituting these into the initial equation (27) we find to a first order in ε the following relation

$$\varepsilon \sum_{m=-\infty}^{\infty} e^{im(\omega t - qk)} \left[m\omega - 2D + 2J\left(\cos mq - 1\right)\right] \Psi_m^{(1)} = 0, \tag{29}$$

assuming that $\Psi_1^{(1)}$ is nonzero, one obtains the dispersion relation

$$\omega = 2D + 2J\left(1 - \cos q\right) \tag{30}$$

and the condition that all $\Psi_m^{(1)}$ with $m \neq 1$ are equal to zero. In the second order we choose the harmonics $e^{i(\omega t - qk)}$ (i.e. the harmonics with $m = 1$) and find

$$\left[\omega - 2D - 2J\left(1 - \cos q\right)\right] \Psi_1^{(2)} + i\left(V - J\sin q\right) \frac{\partial \Psi_1^{(1)}}{\partial \xi} = 0. \tag{31}$$

Taking into account the dispersion relation (30) one arrives at the relation for the soliton velocity

$$V = 2J\sin q. \tag{32}$$

In the third order approximation, we collect the harmonics with $m = 1$ and obtain

$$-\left[\omega - 2D - 2J\left(1 - \cos q\right)\right] \Psi_1^{(3)} - i\left(V - 2J\sin q\right) \frac{\partial \Psi_1^{(2)}}{\partial \xi} + i\frac{\partial \Psi_m^{(1)}}{\partial \tau} - J\cos q \frac{\partial^2 \Psi_m^{(1)}}{\partial \xi^2} - \left[D + J\left(1 - \cos q\right)\right] \Psi_m^{(1)} \left|\Psi_m^{(1)}\right|^2 = 0.$$

Thus, taking into account (30) and (32) the nonlinear equation has the form

$$i\frac{\partial \Psi_1^{(1)}}{\partial \tau} - J\cos q \frac{\partial^2 \Psi_1^{(1)}}{\partial \xi^2} - \frac{\omega}{2} \Psi_1^{(1)} \left|\Psi_1^{(1)}\right|^2 = 0. \tag{33}$$

In full analogy with the dipolar case, one soliton solution of this equation has the form

$$\Psi_1^{(1)} = \exp\left[-i\frac{\omega}{4}\tau\right] \Big/ \cosh\left[\xi\sqrt{\frac{\omega}{4J\cos q}}\right], \qquad s_k^+ = \varepsilon \exp\left[-i\frac{\omega}{4}\varepsilon^2 t\right] \Big/ \cosh\left[\varepsilon(k - Vt)\sqrt{\frac{\omega}{4J\cos q}}\right]. \tag{34}$$

Defining the soliton amplitude $B = \varepsilon$ we recover the second expression appearing in the main text under Eq.(5) with definitions Eqs.(7,8).